Review

# Study of impact on helicopter blade

I. Tawk [a], J. Aubry [b], P. Navarro [b], J.-F. Ferrero [c,*], S. Marguet [c], S. Rivallant [b], S. Lemaire [d], P. Rauch [d]

[a] University of Balamand, Deir El-Balamand, El-Koura, Lebanon
[b] Université de Toulouse/ICA/ISAE, 10 av., E. Belin, 31055 Toulouse Cedex, France
[c] Université de Toulouse/ICA/UPS, 118 Rte de Narbonne, 31062 Toulouse, France
[d] Eurocopter Marignane/BDD, Aéroport Marseille P., 13725 Marignane, France

ARTICLE INFO

*Keywords:*
Composite
Impact
Finite element analysis
Damage assessment

ABSTRACT

This article presents a study of damage in structures that are similar to helicopter blade sections, subjected to an impact. These complex composite structures were impacted by a steel ball of 125 g at impact speed ranging from 30 to 130 m/s. This led to properly highlight the kinematics of the impact and to define the sequence of the damage's mechanisms. An explicit FE model is also presented. The damage modelling of the roving is performed through a scale change. It allows a good representation of observed experimental behaviour. As the mesh density is low, it can be used for the modelling of a real structure.

## 1. Introduction

To reduce certification and development costs, computational methods are required by the aeronautical industry that are able to predict the structural integrity of composite structures under impact from various bodies, such as birds, hailstones, small metal parts and other soft or hard objects.

The complexity of impact problems is increased when composite materials are involved, due to the distinct failure mode that may occur. The comprehensive review by Abrate [1–3] discusses impact failure mechanisms and summarises impact modelling approaches, based mainly on analytical models.

Recent advances in understanding the damage mechanisms of laminated composite [4–9] coupled with development of the performance and capability of computers, offer the possibility of avoiding many experimental tests by using impact simulation. However, numerical results should be examined cautiously. They must, in addition, be validated by experimental tests. A key point in this research is the development of models that are usable in an industrial structure modelling.

The objective of this study is to propose a methodology of calculation that can be used by industry for the analysis of a rigid body impact on complex composite structures such as helicopter blades. Very few impact studies have been conducted on complex composite structures. They deal generally with soft body impact, such as gelatine, hail or ice [10–12].

In this study, impact tests on structures similar to the blade sections are performed. They are carried out using a steel ball and for a wide range of speed. These tests allow the identification of the kinematic mechanisms of degradation. Following this, a model is proposed which represents the observed experimental phenomena. It relies on a multi scale approach. Some models of realistic damage that can be used on industrial structures are proposed. The numerical model is validated by comparison with experimental results.

* Corresponding author. Tel.: +33 5 6155 8645; fax: +33 5 6155 8178.
*E-mail address:* Jean-Francois.Ferrero@isae.fr (J.-F. Ferrero).

## 2. Experimental test

As shown on the schema, the studied specimens are composed of a main spar with unidirectional glass–epoxy, a skin, a rib with hybrid composite glass–epoxy and carbon–epoxy, a polyurethane foam core, and a protective stainless steel that covers the front edge (see Fig. 1). The length of the specimen was 378.2 mm, and with a maximum thickness of 22 mm.

The tests were conducted using a gas gun. The projectile used was a steel ball with a diameter of 30 mm and a mass of 110 g. This steel ball was stabilized inside the gas gun by a polyurethane foam support. The impact speed was regulated by controlling the gas pressure. The specimen was positioned inside a safety box. A Fastcam Photron camera with high capacity was used to record the moment of impact. The recording speed used was 30,000 fps (frame per second). Fig. 2 summarises the impact characteristics and the energy balance established (impact energy, energy of the specimen and of the ball after impact, and energy absorbed by the specimen).

The energy absorbed by the specimen during the impact varied between 71% and 76% of the energy provided by the projectile. The time of contact between the projectile and the specimen varied between 0.15 ms and 2.35 ms. The analysis of the pictures obtained with the fast camera during a test can be used to define the kinematics of the impact. The photographs in Fig. 3 present the impact test for a specimen with 550 J. The time between two images was $6.66 \times 10^{-5}$ s.

The projectile impacted the specimen and penetrated into the front edge. Firstly, the shockwave formed at the impact point and spread transversally. After contact with the rib, it then propagated along the length of both ends of the blade. This spread varied with impact energy and corresponded to the separation of the skins from the foam. The time that the spread took to arrive at the edges of the blade was 0.5 ms. The indentation caused a strong plastic deformation of the stainless steel protection which opened and lead to the separation of the skin from the foam. This phenomenon was due to a rupture of a small thickness of the foam bonded with the skin. The observed bending of the front edge decreased after 0.5 ms due to the elastic return of the structure. The experimental tests carried out allowed an understanding of the observable degradations on the test specimens after impact. The depth of the penetration, as well as the deformation of the front edge, was measured using a three-dimensional measurement machine (DEA–Hexagon Metrology). These measurements give the depth, as well as the length, of residual deformation (see Fig. 4). The behaviour is quasi linear for all tests. To quantify the zone of delamination, a tapping was carried out on the two faces of the test specimens. Fig. 5 shows the evolution of the delaminated area as the impact energy increased. In order to analyse the internal damage of the structure, the test specimens were stabilized by inclusion in a resin, and then cut every 10 mm in parallel to the symmetry plane. The observation of the cross sections located in the plane of impact allows the determination of the damage that appears after the degradation mechanism (see Fig. 6).

For an impact energy of 20 J, the damage generated in the structure is limited to a light staking under the impact point of stainless steel protection. When the speed of the projectile increases, it penetrates increasingly into the leading edge of the blade. This results in a plastic deformation of the stainless steel protection, as well as a greater degradation of the roving. Following this, the rupture of the skin/foam interface is initiated by the debonding of the interface between skin and the roving. It is necessary to reach an energy of 500 J to observe a separation between the stainless steel protection and the skin. This separation remains only in the zone impacted by the projectile and does not propagate longitudinally.

The skins are partly or completely torn behind the stainless steel protection throughout the length of the specimen. In this zone, to pass under the stainless steel protection, the skin undergoes a strong localised curvature that can have an influence on the behaviour observed.

For a relatively low energy level, the roving is fissured at the point of impact. For an impact energy of 200 J, the first cracks appear at 45° from the direction of impact. By increasing the impact velocity, the number of cracks in the resin increase while following the same angle. Packages of fibres will move according to this gliding plane. This kinematics of displacement is found for all the impacted blades. For an impact greater than 800 J, localised micro-cracking of the resin and displacement of fibre packages located on the front of the spar are observed. More cracks appear on the rear end of the roving, which causes the complete rupture of the spar. The foam in contact with the spar is also significantly damaged.

The damage observed for cross sections located slightly further from the plane of impact confirms these observations. For impacts greater than 300 J, the energy is sufficient to debond the skins of the roving up to the end of the test specimen. Micro-cracking of the resin and rupture of the fibre plies is limited to the zone located at the impact point. However, debonding can propagate longitudinally and can reach the ends of the specimens.

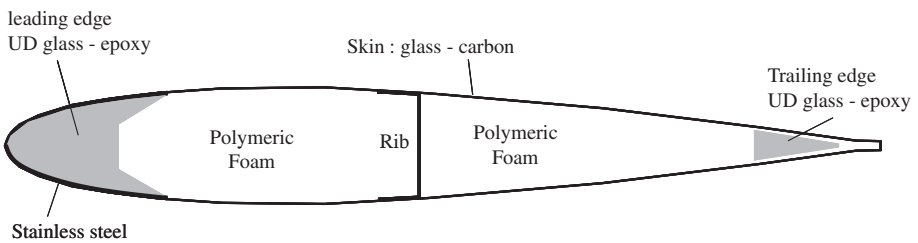


**Fig. 1.** Section of the specimens and materials used.

| Mass specimen (g) | Mass projectile (g) | Impact speed (m /s) | Impact Energy (J) | Specimen energy after impact (J) | Ball energy after impact (J) | Energy absorbed (%) |
|---|---|---|---|---|---|---|
| 437.7 | 121.3 | 18.34 | 20.42 | 5.47 | 0 | 73.2 |
| 440.9 | 124.6 | 49.52 | 152.77 | 41.91 | 0 | 72 |
| 440 | 122.7 | 62.02 | 235.98 | 58.45 | 0.3 | 75 |
| 431.6 | 121.5 | 70.71 | 303.74 | 84.8 | 2.2 | 72.8 |
| 421 | 122.4 | 94.45 | 545.95 | 126.35 | 8.24 | 75.4 |
| 431 | 121 | 119 | 855 | 194.6 | 9.6 | 76 |
| 439.2 | 121.7 | 128 | 997 | 279 | 7.6 | 71.2 |
| 440.4 | 121 | 137 | 1144 | 830.1 | 8.8 | 73.4 |

**Fig. 2.** Characteristics of impact tests.

## 3. Numerical modelling

An F.E. model of the impact on the blade's structure was developed. It must represent the physical phenomena observed in experimental tests. One difficulty results in the compromise between mesh sizing and convergence/calculation time. This can be very limiting for the modelling of the complete blade. The complexity of the phenomena that must be modelled and the scales distinct to which the phenomena of damage appear, force the use of very fine meshing to obtain an acceptable modelling, which involves prohibitive calculation times.

It is then important to set up effective strategies of modelling, with a macroscopic scale, which enable the modelling of these phenomena without the use of fine mesh. These developments were performed using an explicit code RADIOSS.

The main originality of the model is in the modelling of the roving. The model has to represent the damage of the matrix (micro-cracking and cracking) and the fragmentation in packages of fibres, whilst maintaining fibres with no damage.The idea was to model the matrix using 3D elements and the packages of fibres using 1D elements with a surface acceptable compared with the observed experimental results ($\phi$ = 0.9 mm). The fibre surface represents 65% of the spar surface, which is a typical percentage of fibre. During an impact, the matrix is damaged independently and the displacement of fibres is managed by slipping and contact between the 1D elements (see Fig. 7).

The impactor was modelled as a rigid body. The resin, as well as the stainless steel protection, was modelled by elastic–plastic properties with isotropic damage. The composite skin was defined by a conventional property of orthotropic shells. The rupture was managed with strain. The modelling of the roving was carried out using a change scale. An equivalent Young modulus of the glass-fibre was obtained by applying the homogenisation laws. An elastic–plastic law, with damage, was used to model the resin. In order to accurately represent the behaviour of the fibres, being quasi linear until the rupture, a bilinear law with damage and with strain rupture was defined. The foam was modelled by a special law, which is able to differentiate between the compression and traction behaviour.

The numerical model (see Fig. 8) was made up of 104,810 nodes, consisting of 53,408 solid elements, 8819 shell elements and 20,509 bar elements. The length of the blade section with a grid was 280 mm. The definition of different interfaces allows the automatic definition of contacts.

## 4. Results and discussion

The analysis of results obtained from the model allows us to understand the kinematics of the impact. Fig. 9 shows the behaviour of the blade section during the impact for an impact energy of 550 J. The penetration of the front edge at the impact point is on the curve as a function of time.

The image at $t$ = 0.06 ms shows the generation of the wave on the front edge caused by the contact with the ball. The amplitude of this wave increased and the wave propagated in the direction of the impact and towards the two ends of

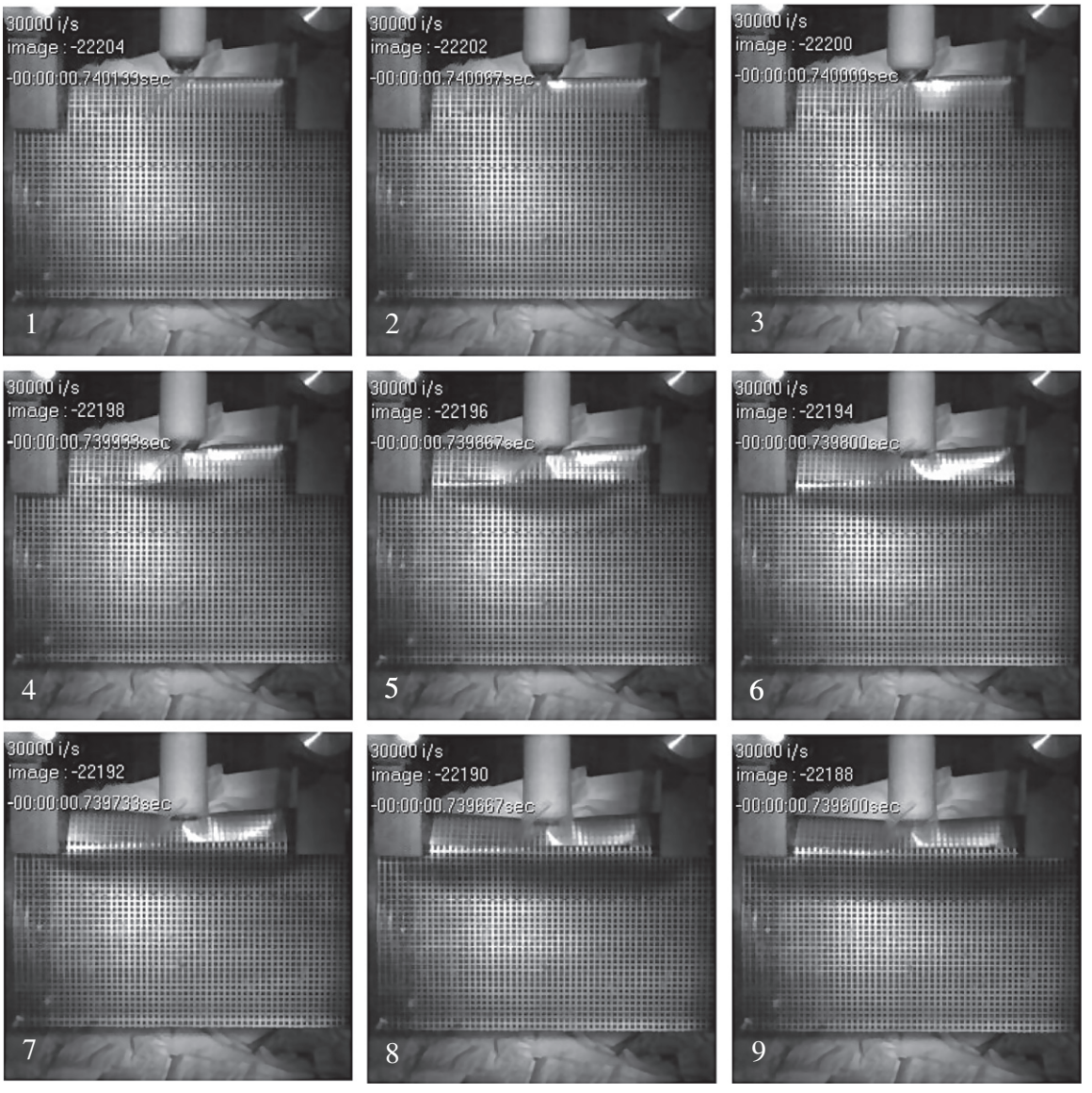


**Fig. 3.** Successive photographs of an impact (67 μs).

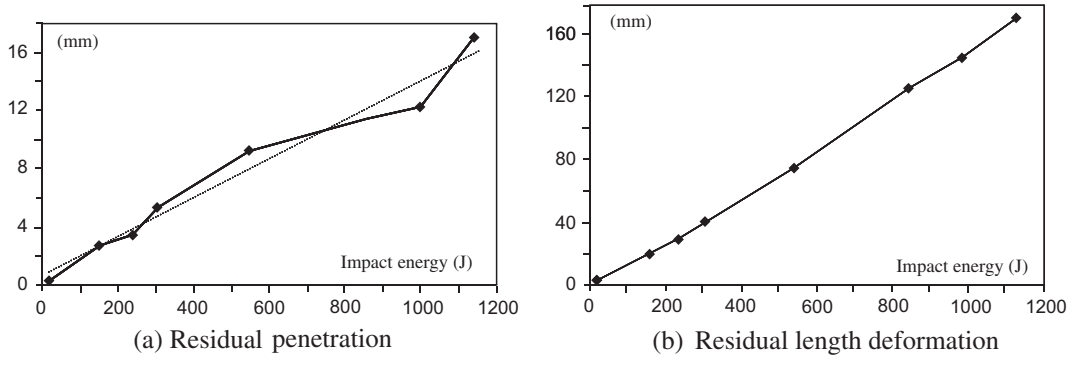


**Fig. 4.** Observable degradation versus impact energy.

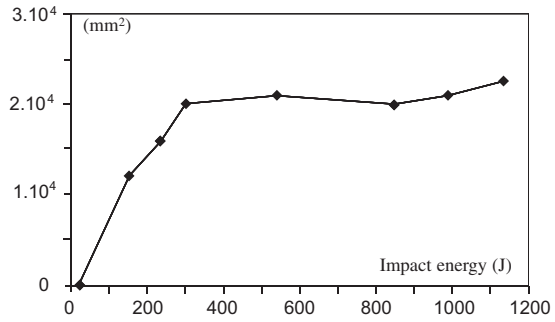


**Fig. 5.** Skin foam debonding versus impact energy.

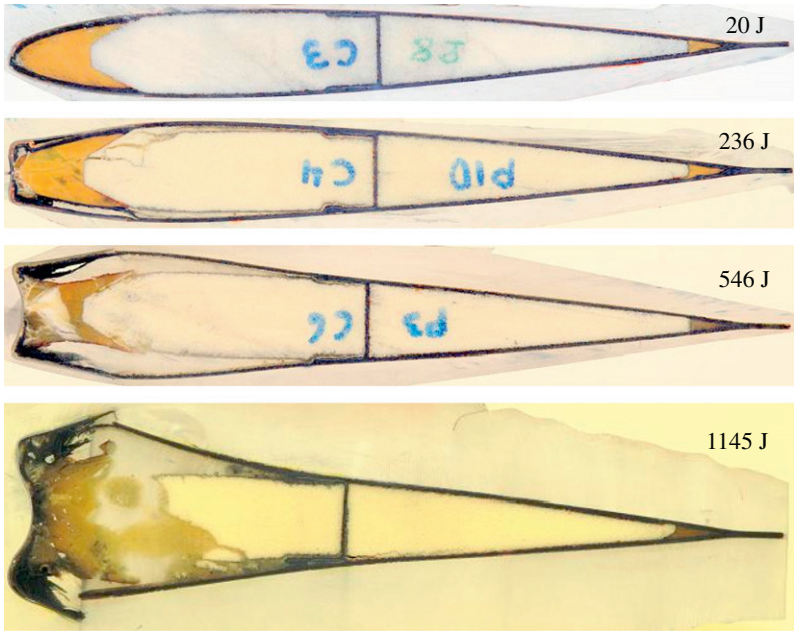


**Fig. 6.** Overview of blade cross section in the plane of impact.

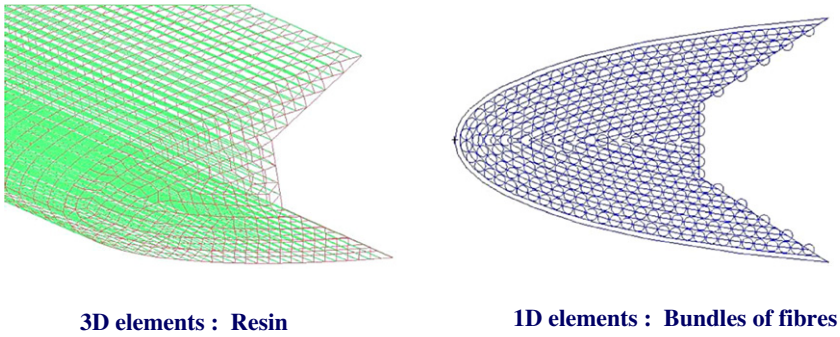


**Fig. 7.** Modelling of the roving.

the blade. This behaviour involved a swelling of the structure and led to delamination at the skin–roving and skin–foam interfaces.

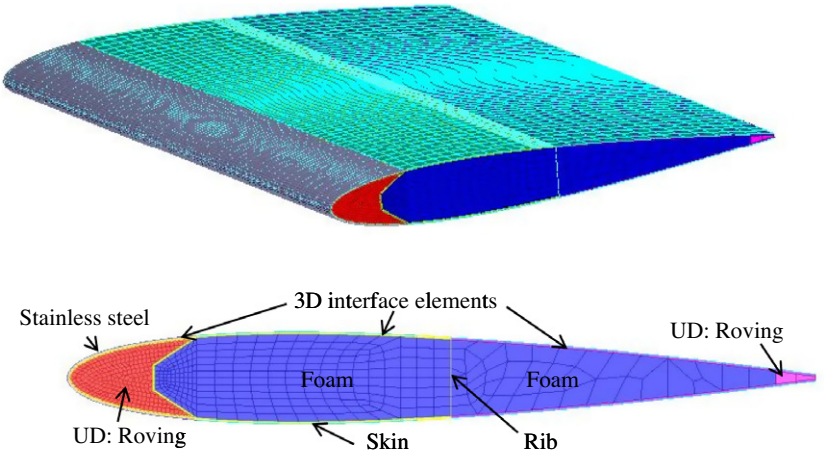


**Fig. 8.** Specimen mesh.

On the graph, which gives the penetration of the front edge as a function of time, four zones can be observed:

- A first zone of load increasing during 0.35 ms, which corresponded to the local phase of damage. The penetration of the ball involved the rupture of the resin, the plastic deformation of the stainless steel protection, and then delamination between the skin and the roving which generated a swelling of the section. The maximum swelling was reached at approximately 0.38 ms.
- A second zone where the penetration of the front edge stabilised for a duration of 0.25 ms. During this time, delamination propagated throughout the entire area between the front edge and the rib.
- A third zone during the next 1 ms which represented the elastic return of the structure.
- A fourth zone where the blade took its final form.

To validate the model, the results obtained numerically were compared with experimental measurements. Fig. 10 shows the speed of the blade after impact (a), the depth of penetration (b), the length of the residual deformation in the front edge (c), as well as the surface of the skin foam debonding as a function of impact energy (d). The results obtained are rather close. The maximum relative error for the blade speed after impact is 8.48%, for an impact energy of 854 J ($V$ = 119 m/s). It is 5.68% for the penetration in the front edge, 4% for the length of residual deformation of the front edge and finally, 7.5% for the delamination area. These results show that the strategy used for the model is valid and that the model provides a good representation of the experimental ruptures for energy levels less than 1000 J. To test the robustness of the model, an impact of 520 J on a specimen with two plies of skin was modelled. The skin was made up of one ply of glass with 0°/90° orientation and one ply of carbon fabric with ±45° orientation. For the experimental test, this specimen was instrumented with strain gauges bonded to the structure in the axis of the impact, on the level of the spar, at the level of the rib and behind the rib.

Graphs (B, N, and D) shown in Fig. 11 presents the strains measured by the gauges and those calculated numerically as well as a zoom for the first 0.5 ms of the impact. This duration represents the time taken for the shock wave to reach the end of the specimen. For the three gauges, the numerical strain results are close to those measured in the experiments. The model reacted in the same way to that of the test specimen. At the beginning of the contact, the slope of the load is identical to that measured in the experiments.

The slope undergoes a break at $t$ = 0.11 ms, which corresponds numerically to the beginning of the delamination at the skin–foam interface behind the spar. The elements of the skin–roving interface were broken and the resin was damaged locally under the impact point. The delamination of the skin–foam interface propagates by rupture of the interface elements, and reaches the rib. This phase corresponds to the unloading of the skin, which in the experiment, resulted in a major reduction in the strains measured by the gauges. This phenomenon is well represented numerically.

If one considers the strains measured behind the rib (D), the behaviour of the strains obtained numerically is very close to that measured in the experiment. When delamination reaches the rib, a decrease in the strains can be observed, which was also observed experimentally.

Upon impact, most of the energy is dissipated at the point of impact by plastic deformation of the stainless steel protection and by damage of the roving. Taking into account this damage is essential in the calculation result. The difficulty is to represent it in a finite element model of the complete structure. The developed strategy provides a solution to this problem. For the roving, the scale of the modelling is not the classical scale related to the material. It is related to the physical phenomena observed experimentally and used to represent the behaviour of the roving during an impact. This type of approach can be developed to represent different types of phenomena (buckling or damage) that appear on a smaller scale than that envisaged for the modelling of an industrial structure.

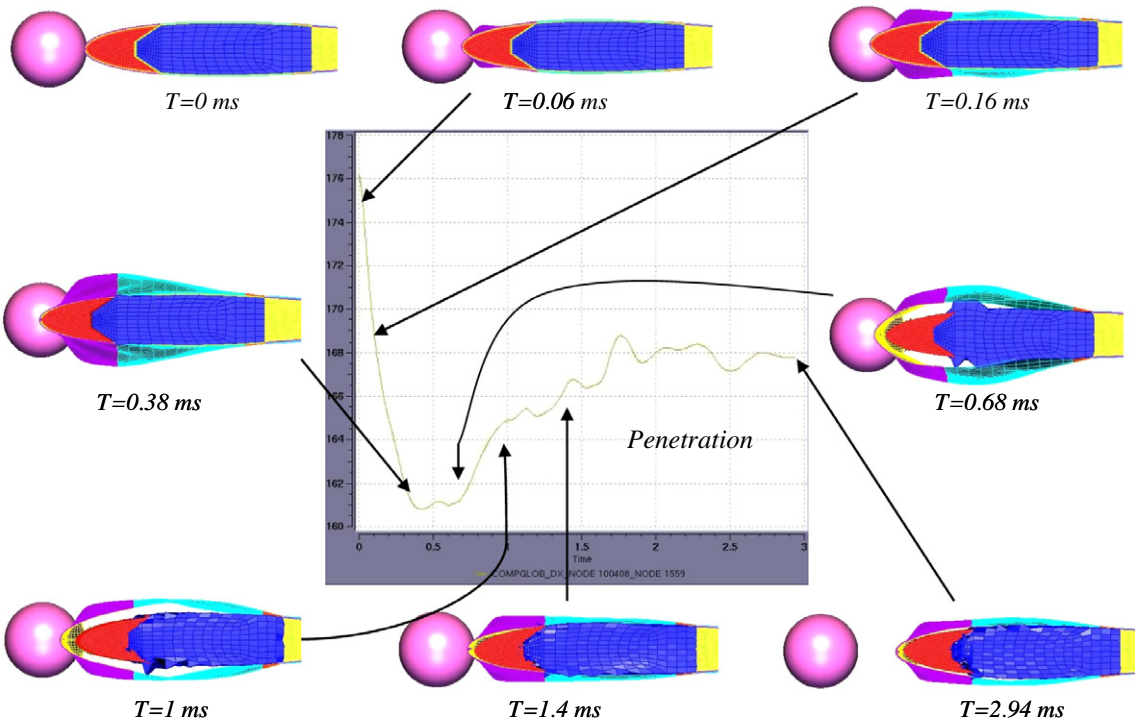


**Fig. 9.** Behaviour of the blade during the impact.

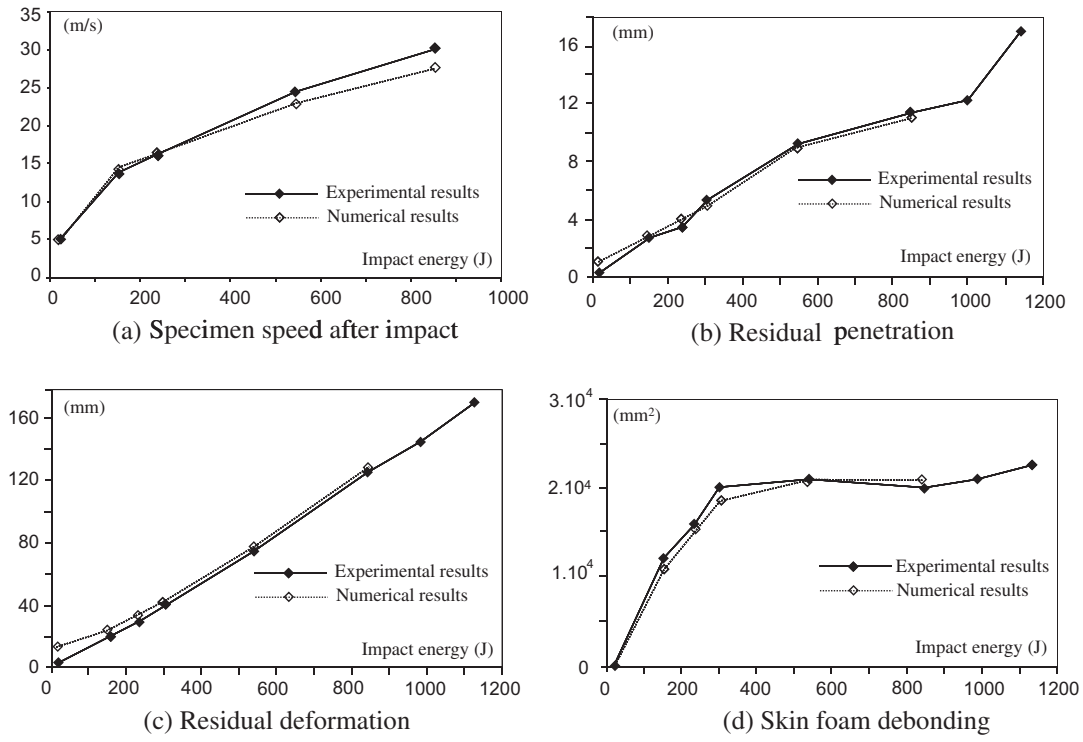


**Fig. 10.** Numerical/experimental results.

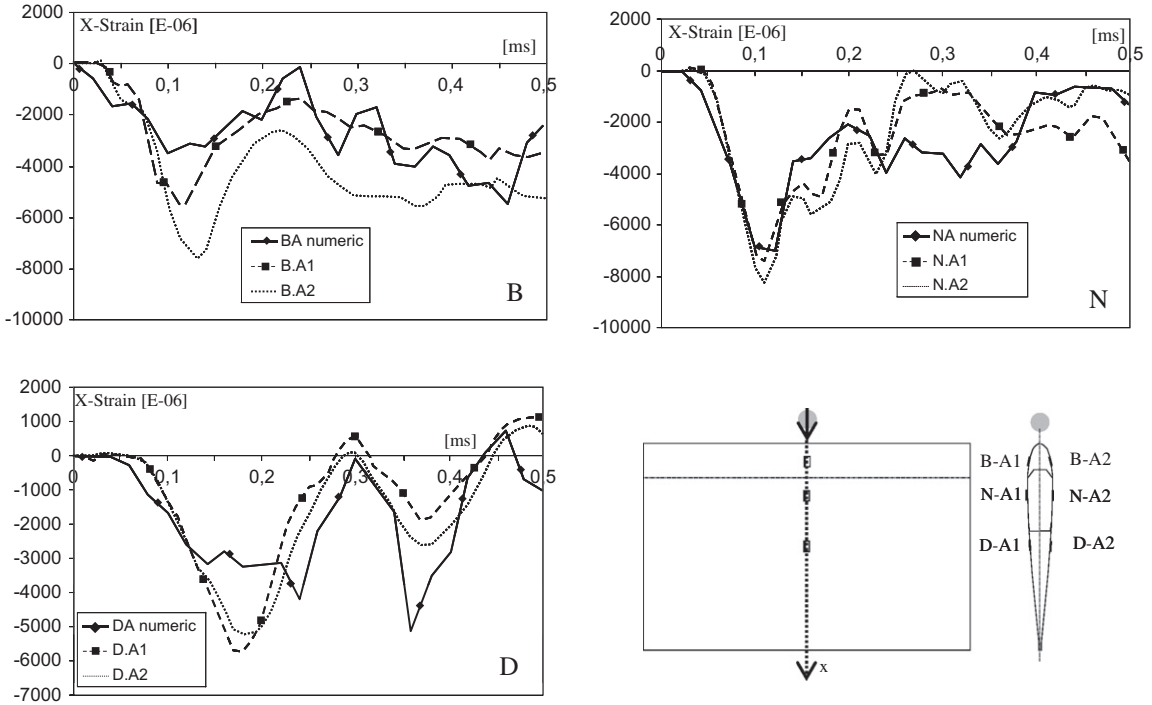


**Fig. 11.** Experimental and numerical strains in the axis of the impact versus time.

## 5. Conclusion

Many experimental tests were carried out to further understand the phenomena concerned during and after a frontal impact to a blade. From the observations, the mechanism of damage could be defined. Firstly, the front edge is the first element that undergoes damage, and then the rise of the impact energy level causes a plastic deformation of the stainless steel protection, which leads to the delamination skin–foam of the structure. Moreover, the penetration of the projectile damages the roving by cracking the resin, which causes the slipping of the packages of fibres on both sides of the impacted zone. A new strategy for the modelling of the impact on blades was proposed. This strategy consists of modelling the roving by the superposition of 3D and 1D elements. The 3D elements represent the epoxy's resin, while the 1D bars represent the packages of fibres. This approach was validated by the results obtained through the modelling of an impact on the blade specimen for various speeds. These results are satisfactory. The developed model allows a good representation of all the experimental ruptures for energy levels less than 1000 J.

The developed method precisely evaluates the energy dissipated by the damage to the roving. It allows this phenomenon to be taken into account in a scale model of the structure without greatly increasing the computing time.

This approach can be used industrially in the phase of pre-dimensioning to model the behaviour of the blade subjected to an impact. The developed model does not take into account the delamination of the two interfaces skin–rib and skin–roving. To manage these phenomena, a specific volume multi-layer element, dedicated to the modelling of the delamination, is currently in development within the team.

## References


[1] Abrate S. Impact on laminate composites. Appl Mech Rev 1991;44:155–90.
[2] Abrate S. Impact on laminate composites, recent advances. Appl Mech Rev 1997;47:517–44.
[3] Abrate S. Impact on composite structures. Cambridge: Cambridge University Press; 1998.
[4] Talreja R. Damage mechanics of composite materials. Composite materials series, 9. Amsterdam: Elsevier; 1994.
[5] Jonhson AF, Pickett AK, Rozycki P. Computational methods for predicting impact damage in composite structure. Compos Sci Technol 2001;61:2183–92.
[6] Hu N, Zemba Y, Okabe T, Yan C, Fukunaga H, Elmarakbi AM. A new cohesive model for simulating delamination propagation in composite laminates under transverse loads. Mech Mater 2008;40:920–35.
[7] Tawk I, Navarro P, Ferrero JF, Barrau JJ, Abdullah E. Composite delamination modelling using a multi layered solid element. Compos Sci Technol 2010;70:207–14.
[8] Tay TE, Liu G, Tan VBC, Sun XS, Pham DC. Progressive failure analysis of composites. J Compos Mater 2008;42:1921–66.
[9] Fleming DC. Delamination modeling of composites for improved crash analysis. NASA CR-1999-209725.
[10] Johnson AF, Holzapfel M. Modelling soft body impact on composites structures. Compos Struct 2003;61:103–13.
[11] Anghileri M, Castelletti LML, Invernizzi F, Mascheroni M. A survey of numerical models for hail impact analysis using explicit finite element codes. Int J Impact Eng 2005;31:929–44.
[12] Kim H, Welch DA, Kedward KT. Experimental investigation of high velocity ice impacts on woven carbon/epoxy composite panels. Composites Part A 2003;34:25–41.